The S_e sensitivity of metals under swift-heavy-ion irradiation: a transient thermal process

1994 J. Phys.: Condens. Matter 6 6733

(http://iopscience.iop.org/0953-8984/6/34/006)

J. Phys.: Condens. Matter 6 (1994) 6733–6750. Printed in the UK

The S_e sensitivity of metals under swift-heavy-ion irradiation: a transient thermal process

Z G Wang†§, Ch Dufour†‡, E Paumier†‡ and M Toulemonde†

† Centre Interdisciplinaire de Recherches avec les Ions Lourds, Laboratoire mixte CEA–CNRS, rue Claude Bloch, Boîte Postale 5133, 14040 Caen Cédex, France

‡ Laboratoire d'Etude et de Recherche sur les Matériaux, associé au CNRS (URA 1317) ISMRa, Université de Caen, 14050 Caen Cédex, France

Received 28 February 1994, in final form 27 April 1994

Abstract. In the framework of the thermal-spike model the present paper deals with the effect of the electronic stopping power (S_e) in metals irradiated by swift heavy ions. Using the strength of the electron–phonon coupling $g(z)$ with the number of valence electrons z as the unique free parameter, the increment of lattice temperature induced by swift-heavy-ion irradiation is calculated. Choosing $z = 2$, the calculated threshold of defect creation by S_e for Ti, Zr, Co and Fe is about 11, 27.5, 28 and 41 keV nm^{-1}, in good agreement with experiment. Taking the same z value, the calculation shows that Al, Cu, Nb and Ag are S_e insensitive. Moreover, in Fe, the differences in the damage created by U ions of different energies but exhibiting the same value of S_e may be interpreted by a velocity effect. Using $z = 2$, other calculations suggest that Be ($S_e \geqslant 11$ keV nm^{-1}), Ga ($S_e \geqslant 5$ keV nm^{-1}) and Ni ($S_e \geqslant 49$ keV nm^{-1}) should be sensitive to S_e but Mg should not. These examples put the stress on the effect of the physical parameters governing the electron–phonon coupling constant apart from z determination: the sound velocity linked to the Debye temperature and the lattice thermal conductivity. Furthermore, a simple criterion is proposed in order to predict the S_e sensitivity of metals.

1. Introduction

It is well established that an energetic ion passing through a solid loses its energy via two nearly independent processes: (i) electronic excitation and ionization (i.e. electronic slowing down S_e, or electronic energy loss $-(dE/dx)_e = S_e$); and (ii) elastic collisions with the nuclei of the target atoms (i.e. nuclear slowing down S_n, or nuclear energy loss $-(dE/dx)_n = S_n$). In high-energy ion–solid interactions, the nuclear energy loss may be neglected as compared to the electronic energy loss, so the present paper will deal with the effect induced in pure metals by the electronic slowing down of swift heavy ions. In fact, the amorphization of $Pd_{80}Si_{20}$ induced by ^{235}U fission fragments observed by Lesueur [1] showed that a high electronic excitation was playing an important role in the volume of a metallic compound. Since that first experiment, a series of other irradiations has been performed in the electronic slowing-down regime on the following metallic materials.

(i) For amorphous (a-) materials, an ion-beam-induced huge plastic deformation has been discovered in a-$Pd_{80}Si_{20}$, a-$Cu_{50}Zr_{50}$, and some other metallic glasses [2–6]: here the incident ion beam acts as a hammer on the samples and this results in a growth perpendicular to the beam direction. It is suggested that the electronic energy loss S_e

§ On leave from the Institute of Modern Physics, Academia Sinica, 253 Nanchang Road, 730000 Lanzhou, People's Republic of China.

0953-8984/94/346733+18$19.50

could provoke substantial atomic displacements and thus could predominantly drive the plastic deformation [4, 5]. The experiments on a-$Fe_{85}B_{15}$ ribbons irradiated with high-energy heavy ions [5, 6] show that, above an S_e threshold value, the electronic energy loss plays a crucial role in radiation-induced damage. Moreover, the whole radiation-induced phenomenon (incubation and growth) is due to the electronic energy-loss effects and the incubation process is connected to the creation of defects.

(ii) For crystalline (c-) materials, swift-heavy-ion-induced amorphization and latent track creation have been observed in c-Ni_3B [7] and c-Ni-Zr [8, 9] alloys: above an S_e threshold, the tracks consist of droplets, which are transformed into continuous cylinders when the level of electronic excitation increases.

(iii) For pure crystalline metals, S_e induces a decrease of defect production efficiency in Ni and in Fe ($S_e < 50$ keV nm^{-1}) [10–17] as well as in FCC FeCrNi alloys [18]. An S_e-induced increase of defect-production efficiency in Bi, Ti, Zr, Co and Fe ($S_e > 50$ keV nm^{-1}) [13, 14, 17, 19–22] is evidenced. Furthermore, it is also shown that S_e-induced phase transition and latent track creation occur in pure Ti [20, 21]. Defect production in Ga was suggested [23] but not clearly confirmed at higher values of S_e [24]. This is probably due to the fact that specific physical properties of different crystallographic phases in Ga [25] could hide the S_e effect.

All these experimental results show that the high electronic excitations can also induce structural modifications in metallic systems similar to those in non-metallic materials [26–28]. This means that all the S_e-dependent effects induced in different materials are probably related to the same basic energy transfer process between the incident ions and the target atoms. Two models of microscopic energy-transfer mechanism, the thermal spike [29–33] and the ionic spike [14–17, 34–36] have been used to try to establish which are the relevant parameters governing the basic energy-transfer process. In the electronic slowing-down regime ($S_e \gg S_n$), most of the energy of the incident ions is transferred to the host electrons, resulting in a high electronic ionization (ionic spike) and/or a high temperature increase of the electronic subsystem (thermal spike). In the course of time, the ionic spike ($\sim 10^{-14}$ s) could be covered by the thermal spike ($\sim 10^{-12}$ s), so the question to be answered is whether the defects finally observed result from the initial atomic motions induced by ionic spikes or are a consequence of a huge local increase of the lattice temperature by the thermal spikes, which could erase the previous atomic motions. In fact, several experiments [13, 14, 17, 20–22] show that the materials with strong electron–phonon (E–P) coupling are sensitive to the electronic energy loss, suggesting that the thermal spike is an ingredient in the damage process. For instance, the crystalline noble metals such as Ag and Cu [17, 37] with a weak E–P coupling are insensitive to S_e. In contrast, the S_e-induced annealing of elastically created point defects in Ni and in Fe [10–17] and the S_e-induced defect creation in Ti, Co, Zr, and Fe [13, 20–22] occur in metals exhibiting stronger E–P coupling than that of noble metals. Crystalline Al and W, which have relatively weak E–P coupling are insensitive to S_e [13, 17, 38]. In the same way, the fact that a-Ni_3B is more sensitive to S_e than c-Ni_3B [39, 40] could be related to the stronger E–P coupling in amorphous states than in crystalline ones. Moreover, a metal such as Bi with low melting point is sensitive to S_e though the E–P coupling is relatively low [19]. As compared to W, the Bi sensitivity shows that the amount of energy necessary to melt it is also a relevant parameter. From all the experimental phenomena quoted above, one can see that the questions are what the relationship is between the S_e-induced effects and the E–P coupling and how to define whether a given material is S_e sensitive or not. Therefore, it is necessary to make a more detailed comparison between theoretical and experimental results in the framework of the thermal-spike model in a series of pure crystalline metals.

According to the thermal-spike model and taking into account the E–P coupling, the energy locally deposited by electronic energy loss in matter is quickly shared among the electron gas by electron–electron interactions and then transferred to the neighbouring atoms by electron–phonon and phonon–phonon interactions. Some considerations on the E–P coupling strength [41, 42] and electronic diffusivity [43] have made it possible to theoretically evaluate the lattice temperature increment in thermal spikes. On the basis of the observations of latent tracks in matter [8, 9, 21], it is assumed in the present paper that a latent track results from rapid quenching of a cylinder of molten matter. The thermal-spike model will be used to calculate the latent-track radii as performed previously with success in a-Si, a-Ge and a-$Fe_{85}B_{15}$ [29, 44, 45].

In section 2, we develop physical considerations leading to the mathematical descriptions of the thermal spike. Input parameters governing the energy diffusion on the electron subsystem and the energy transfer to the lattice [12, 41, 42, 46–48] will be presented. In section 3, the results of the calculation performed for several metals (Ti, Zr, Co, Fe, Al, Cu, Nb, Ag, Pt, Pd, Ni, Bi) are compared to the S_e thresholds of defect creation. The comparison is extended to latent track radii deduced from analysis [22] of experimental data of defect creation. The ion velocity effect is proposed to explain the results obtained in Fe [16]. According to these comparisons, we predict in section 4 the behaviour of other metals (Be, Ga, Ni). In conclusion, a criterion is defined to predict the S_e sensitivity of metals, especially the transition metals.

2. Numerical calculations

2.1. Physical considerations

According to the energetic ion–solid interactions, high-energy heavy-ion irradiation is able to induce a high density of electronic excitations in solids along the ion path. Then the problem is to quantify the effects of the electronic energy relaxation that results from the electron–electron and electron–atom interactions. Following the previous descriptions [31, 32], we assume that this process is described mathematically by two coupled differential equations governing the energy diffusion in the two subsystems (electron and lattice) and their coupling. Several experiments on metals irradiated by fs laser pulses [46, 47, 49–52] support such a description, since there is a good correlation between the theory and experiments [46]. As radiation defects created in materials by highly energetic ions are cylindrical [8, 9], a time-dependent thermal transient process is expressed in cylindrical geometry [32]

$$C_e(T_e)\partial T_e/\partial t = \nabla(K_e(T_e)\nabla T_e) - g(T_e - T) + A(r,t) \tag{1a}$$

$$C(T)\partial T/\partial t = \nabla(K(T)\nabla T) + g(T_e - T) \tag{1b}$$

where T_e, T, C_e, C and K_e, K are the temperature, the specific heat and the thermal conductivity for the electronic and atomic systems respectively, $A(r,t)$ is the energy density per unit time supplied by the incident ions to the electronic system at radius r and time t such that $\int\int 2\pi r A(r,t)\,dr\,dt = S_e$ and g is the E–P coupling factor. As these parameters are temperature dependent, the coupled differential equations are non-linear and can be only numerically solved. Using the numerical analysis proposed in [45], the lattice temperature $T(r,t)$ at each time t and radius r is calculated. Taking into account the latent heat of fusion when the lattice temperature reaches the melting point, the radii of molten cylinders induced by energetic ions can be deduced.

In such a description, questions arise: can we define the temperature in such a short time? Can we ignore the pressure dependence of the different physical parameters of the lattice? The purpose of the present paper is not to discuss these two points in detail but to give some support to the use of the equilibrium thermodynamic parameters. Indeed, the thermalization of the highly energetic electrons at the Fermi level occurs in a very short time [53] (of the order of 10^{-15} s) as shown by high-power fs laser experiments [54]. The thermalization of the lattice occurs only in a time of 10^{-13} s, which is larger than the inverse of the usual Debye frequency [48]. Consequently we shall assume that for times below 10^{-13} s the calculated lattice temperature represents only the energy deposited on the atoms. The effect of the pressure dependence of the melting point was previously discussed [19, 29]. As no trends due to this effect were observed within the experimental errors [26] and within the uncertainties of the input parameters in the calculation [29], we shall neglect it in the present calculations.

2.2. *Main physical quantities*

For pure metals, lattice thermal conductivity $K(T)$, specific heat $C(T)$ and latent heats of fusion and vaporization are well known from practical measurements [55–58] (see the appendix, tables A1 and A2). The parameters entering the equations governing the energy diffusion on the electron subsystem are described by supposing the electrons behave like quasifree electrons in a noble metal while the E–P coupling is described by taking into account the physical properties of the irradiated material.

2.2.1. The energy density per unit time $A(r, t)$. According to the delta-ray theory in energetic ion irradiation [59], the radial energy deposition may be described as

$$A(r,t) = bS_e \exp(-(t-t_0)^2/2\sigma_t^2)F(r). \tag{2}$$

t_0 is the mean flight time of the delta-ray electrons [60] and is of the order of 10^{-15} s, t_0 can be chosen in the range 10^{-15}–5×10^{-15} s without any influence on the radius of the molten zone [45]. The half width of the Gaussian distribution σ_t is assumed to be equal to t_0. $F(r)$ is a spatial distribution function of delta-electron energy deposition in matter, which has been given by Waligorski *et al* [61], and b is a normalization constant:

$$\int_{t=0}^{\infty}\int_{r=0}^{r_m} bS_e \exp\left(-\frac{(t-t_0)^2}{2\sigma_t^2}\right) F(r)2\pi r\,dr\,dt = S_e.$$

r_m is the maximum projected range of electrons perpendicular to the ion path.

2.2.2. The electronic specific heat $C_e(T_e)$. In the free-electron-gas theory [48], the electronic specific heat C_e of a metal is given as a linear function of T_e: $C_e = \gamma T_e = (\pi^2 k_B^2 n_e/2E_F)T_e$ for low values of T_e. The Fermi energy is given by $E_F = (\hbar^2/2m_e)(3\pi^2 n_e)^{2/3}$, where m_e is the electron mass, n_e is the electron number density and k_B and $\hbar$ are Boltzmann and Planck constants respectively. The specific heat will follow this linear law up to the Fermi temperature $T_F = E_F/k_B$ above which C_e becomes a constant ($C_e = \frac{3}{2}k_B n_e$) [48].

2.2.3. The electronic thermal conductivity $K_e(T_e)$. The $K_e(T_e)$ evolution was discussed previously [19, 62] and determined from an experimental scaling of the thermal diffusivity $D_e(T_e)$ with respect to Au, a noble metal in which the electrons behave like a quasifree-electron gas ($K_e(T_e) = C_e(T_e)D_e(T_e)$). In the present case, the scaling values were $D_e(300\ \text{K}) = 150\ \text{cm}^2\ \text{s}^{-1}$ and $D_{min} = 4\ \text{cm}^2\ \text{s}^{-1}$ [43] for all the selected metals.

2.2.4. The electron–phonon coupling g. If the lattice temperature is not much smaller than the Debye temperature T_D [41, 42], the g factor may be approximately expressed as

$$g = \frac{\pi^2 m_e n_e v^2}{6\tau_e(T_e)T_e} \tag{3}$$

where $\tau_e(T_e)$ is the electron mean free time between two collisions at temperature T_e and v is the speed of sound in the metal, linked to the Debye temperature T_D and the atomic number density n_a by $v = k_B T_D/\hbar(6\pi^2 n_a)^{1/3}$. The determination of $\tau_e(T_e)$ is indeed very difficult. To bypass this difficulty, we have related $\tau_e(T_e)$ to the electrical conductivity $\sigma_e(T_e)$ [48] of the metal under study [56] and then

$$g = \frac{\pi^4 (k_B n_e v)^2}{18 L \sigma_e(T_e) T_e}. \tag{3'}$$

L is the Lorentz number. Using the Wiedemann–Franz law $K_e(T_e) = L\sigma_e(T_e)T_e$, g can be related also to the thermal conductivity

$$g = \frac{\pi^4 (k_B n_e v)^2}{18 K_e(T_e)}. \tag{3''}$$

As previously [19], the g factor will be evaluated versus the temperature using the measured values of the thermal conductivity of the metal under study. This means that we assume that $K_e(T_e) = K(T)$ in order to take into account the specific properties of the irradiated metal under consideration (see the appendix, table A2).

2.3. Calculations

According to the basic considerations shown above, the temperature responses of electronic and atomic systems to various S_e and different ion energies have been calculated taking into account the temperature dependence of the lattice parameters (see the appendix). In these simulations, the unique free parameter for the selected pure metals is the valence electron number z (the electronic density is $n_e = zn_a$, n_a being the atomic density). The uncertainty of the calculation results is linked to the uncertainty of the input parameters.

Using the equations (3′) and (3″) either with the experimental electrical resistivity $\rho_\mu (= \sigma_e^{-1})$ or thermal conductivity at room temperature (table 1), one can estimate in a first approximation that the $g(z)$ factor for $z = 1 (= 2)$ is known within 15% (30%). The results of the calculation are directly linked to the S_e input. Figure 1 shows the S_e determinations from different calculations using different approximations [16, 63, 64]. The error in the S_e value is around 10%, but for light targets (e.g. Be) it may be as high as 50% at the Bragg peak [63, 65]. However, we shall assume that S_e is known within 10%. Taking into account all these uncertainties, 30% discrepancies between the calculated and the experimental results will be considered as acceptable.

From the temperature increments of electronic and atomic systems, we obtain the relationship between the input electronic stopping power S_e and the maximum temperature $T_{am}(r)$ reached by the lattice at a distance r from the cylinder axis. For all the calculations, the initial temperature of the sample was 10 K except when a specific temperature is quoted. Figure 2 shows a primary result of the calculation in Ni with the parameters $g(z = 2)$, $S_e = 73$ keV nm^{-1} and incident energy $E_{in} = 5$ MeV amu^{-1}: the temperature of the electronic system increases during a time equivalent to the deposition time ($\sim 10^{-15}$ s). Then the lattice temperature increases mainly because of the E–P interaction. The maximum lattice temperature is reached when both systems are in equilibrium at a mean time equal to

Table 1. Some constants of selected metals at room temperature. T_D, n_e, K and ρ_μ are Debye temperature, electronic density, thermal conductivity and resistivity respectively. The E–P coupling g_{ρ_μ} and g_K values are deduced from equations (3′) and (3″) with $z = 1$.

Metal	T_D (K)	$n_e(z=1)$ (10^{22} cm^{-3})	K (300 K) (W cm^{-1} K^{-1})	ρ_μ (300 K) ($\mu\Omega$ cm)	g_K[a] ($\times 10^{10}$) (W cm^{-3} K^{-1})	g_{ρ_μ}[a] ($\times 10^{10}$) (W cm^{-3} K^{-1})
Be	1440	12.1	2.00	3.76	722	741
Mg	400	4.30	1.67	4.51	16.8	17.3
Al	428	6.02	2.30	2.733	21.9	18.8
Ti	420	5.66	0.22	42.7	203	260
V	380	7.22	0.28	20.2	183	139
Cr	630	8.33	0.94	12.7	179	291
Mn	410	8.15	0.08	144	864	1358
Fe	470	8.47	0.803	9.98	119	130
Co	445	8.97	1.00	6.34	92.6	80.0
Ni	450	9.14	0.91	7.20	107	95.4
Cu	343	8.45	4.01	1.725	12.7	12.0
Ga	320	5.10	0.41	13.65	55.0	42.8
Zr	291	4.29	0.169	43.3	87.6	87.5
Nb	275	5.56	0.54	16.0	34.6	40.8
Pd	274	6.80	0.72	10.80	33.7	35.7
Ag	225	5.85	4.00	1.629	3.34	2.97
Sn	200	3.70	0.67	12.6	8.57	9.87
W	400	6.30	1.69	5.44	27.6	34.6
Pt	240	6.62	0.72	10.8	24.9	26.5
Au	165	5.90	3.17	2.271	2.30	2.26
Pb	105	3.30	0.353	21.3	3.85	3.95
Bi	119	2.84	0.08	117	17.8	23.2
U	207	4.80	0.275	25.7	31.6	30.5

[a] If $z \neq 1$, then $n_e(z) = zn_a$ and $g(z) = z^2 g(z = 1)$.

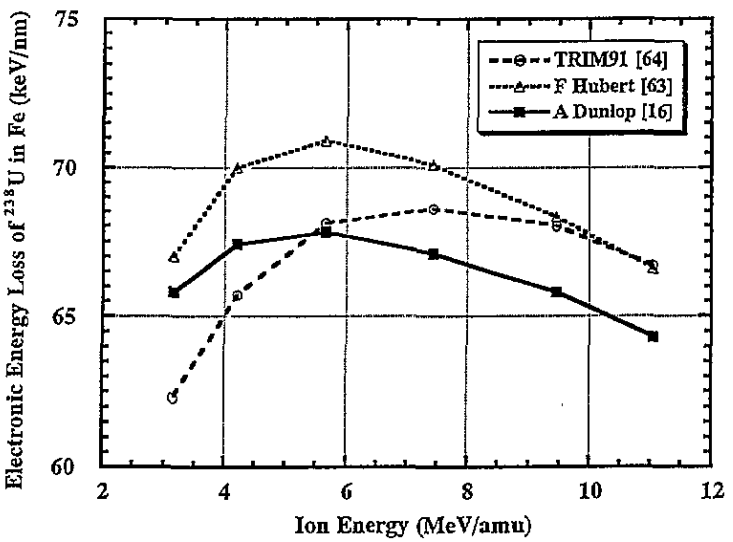

Figure 1. The evolution of the electronic stopping power of an Fe target as a function of the energy of an incident U ion: a comparison between three calculations [16, 63, 64].

$C_e(T_e)/g(T_e)$. After that time, both temperatures decrease and are governed by the thermal conductivity. The molten phase is quenched with a rate of the order of 10^{15} K s^{-1}. The same feature appears when the calculation is performed on other metals. As an example the primary result is given for Cu (figure 3), which is known to be insensitive to S_e. The maximum temperature for Cu is in agreement with previous determinations [31,32]. In such a model a sensitive material will be defined as a material in which the molten phase appears above a threshold value $S_{e_{cr}}$ lower than the maximum value of S_e reached in the case of the U beam. We define the calculated track radius R_m as the maximum cylinder radius in which the molten phase is created.

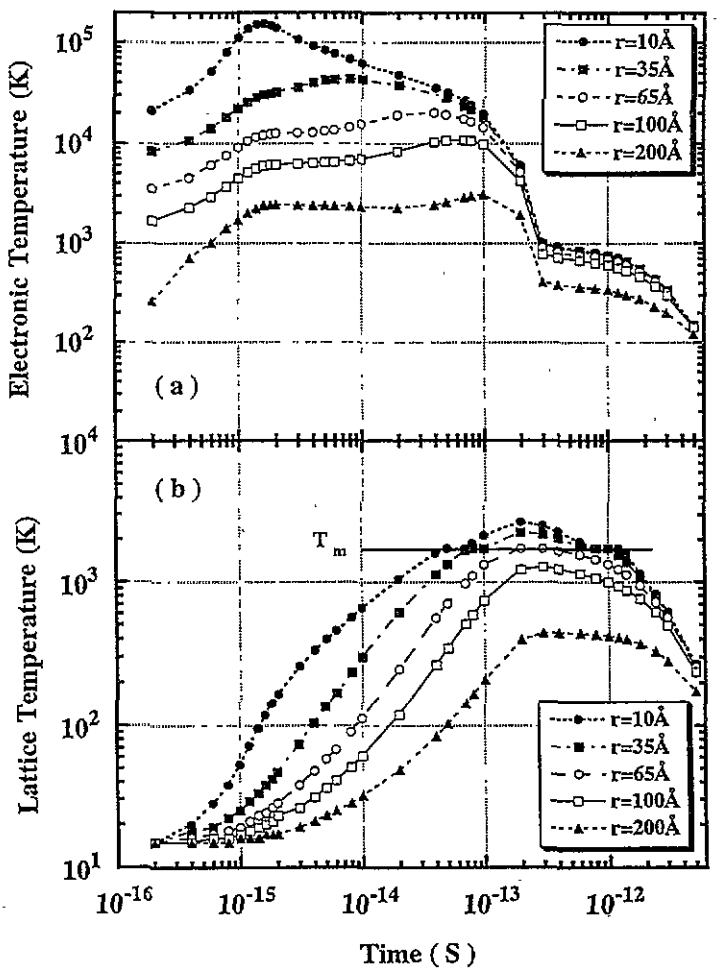

Figure 2. Evolutions of the electronic and lattice temperatures of Ni as a function of time at several radii from the ion path. Here, the initial target temperature is $T_0 = 15$ K and the E–P coupling factor of Ni is $g = g(z = 2) = 4.05 \times 10^{12}$ W cm^{-3} K^{-1} at 300 K. The incident energy is $E_{in} \approx 5$ MeV amu^{-1} and the electronic energy loss is $S_e = 73$ keV nm^{-1}. The symbols indicate at which radius the temperature is calculated.

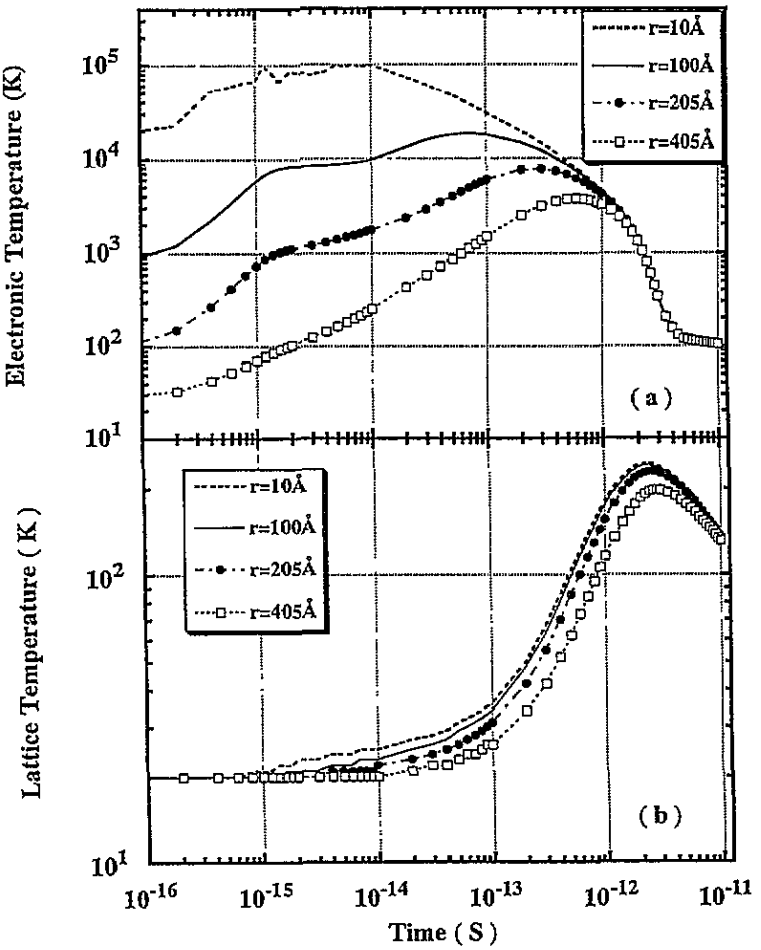

Figure 3. Evolutions of the electronic and lattice temperatures of Cu as a function of time at several radii from the ion path. Here, the initial target temperature is $T_0 = 20$ K and the E–P coupling factor of Cu is $g = g(z = 1) = 1.25 \times 10^{11}$ W cm^{-3} K^{-1} at 300 K. The incident energy is $E_{in} = 5$ MeV amu^{-1} and the electronic energy loss is $S_e = 70$ keV nm^{-1}. For the symbols see the caption of figure 2.

3. Comparison with experiments

In this section, we will perform calculations on S_e-sensitive metals such as Ti, Zr, Co and Fe [13–17, 20–22]. The Bi case was previously treated [19]. Three different points of view will be considered: (i) the threshold $S_{e_{cr}}$ of S_e-induced defect creation in metals; (ii) the track radii and (iii) the ion-velocity effect. At the end, using the results obtained on the sensitive metals, the calculation will be extended to insensitive materials.

3.1. Threshold of defect creation in metals

For each metal Ti, Zr, Co, Fe and Bi, table 2 shows the E–P coupling constant g at 300 K for $z = 2$. Within 30% uncertainties of input parameters (as discussed in subsection 2.3), the calculated thresholds $S_{e_{cr}}$ are in very good agreement with the experimental ones. For all these metals, the $g(z = 2)$ value has been used. It is worth noting that $z = 2$ corresponds

to the electronic density of the considered transition metals [48]. However, this number of excited electrons per atom is still uncertain since a lower value of z has to be used in Bi [19]. In the following, we assume that $z = 2$.

Table 2. A comparison of theoretical and experimental defect creation thresholds $S_{e_{cr}}$ values of some S_e-sensitive metals. The calculated $S_{e_{cr}}$ values are from $g(z) = g(z = 2)$ for the corresponding range of incident ion energies E_{in}. S_e gives the maximum value that can be reached in the irradiations.

Metal	g ($\times 10^{11}$) (W cm^{-3} K^{-1})	E_{in} (MeV amu^{-1})	$S_{e_{cr}}$ (calculated) (keV nm^{-1})	$S_{e_{cr}}$ (measured) (keV nm^{-1})	S_e (TRIM91) (keV nm^{-1})
Ti	92.8	3–20	11–14	<15 [13]	42
Fe	49.8	4–20	41–49	~40 [13]	70
Co	34.5	5–20	28–34	30–40 [13]	75
Zr	35.0	5–20	27.5–31	25–35 [13]	48
Bi	8.20	7–30	11–13	17–24 [19]	50

3.2. Track radii

Before comparing experimental and calculated track radii (R_{exp}, R_{cal} respectively), we must point out that the deduction of experimental radii is strongly dependent on the analysis. R_{exp} is determined from the *in situ* resistivity measurements using a phenomenological model. Keeping in mind this main assumption, we can look at the results in Ti, Zr, Co and Fe (figure 4(*a*)–(*d*) respectively). Considering the uncertainties of input parameters (30%), we find quite a good agreement between the theoretical radii and the experimental radii deduced from the experimental annealing cross section [16, 22] except for one point in Ti. The evolution of R_{cal} versus S_e is shown for several incident ion energies in the range of 3–20 MeV amu^{-1}. It is important to remark that with only one free parameter (the valence-electron number z, taken equal to two for the considered metals), we can find a good order of magnitude of the track radii by taking into account the experimental thermal characteristics of each metal.

3.3. Ion velocity effects

In figure 4(*d*) we observe that for a given S_e, several experimental track radii are shown. This is due to the fact that the same S_e value can be reached in two cases: (i) for a given ion at different velocities in MeV amu^{-1} as we can see in figure 1 and (ii) for different ions at different velocities (see [65]). This velocity effect has been clearly shown in insulators such as $Y_3Fe_5O_{12}$ [27]. We find the theoretical explanation in the works of Waligorski *et al* [61] and more recently Gervais [60]: the higher the ion velocity, the larger the maximum range (r_m) of delta electrons and consequently the lower the deposited energy density. Experimentally for Fe (figure 4(*d*)), the largest track radii correspond to the lowest values of ion velocity (i.e. the highest deposited energy density). In our calculations, this effect is taken into account in the expression of $A(r, t)$ (see subsection 2.2) in which $F(r)$ is the initial spatial energy distribution depending on E_{in}. $S_{e_{cr}}$ is sensitive to the input beam energies (figure 4). For Fe, the curves (figure 5) show the velocity effect in agreement with the experiment, i.e., the radii corresponding to the same S_e value decrease when ion energy increases. The case of Ni must be mentioned here. It has been irradiated with about 1 MeV amu^{-1} ^{127}I ions [10] and 10 MeV amu^{-1} Pb ions [17]. It is shown that a defect annealing appears at a lower S_e value for the irradiation performed by Iwase *et al* [10–12] as compared to the ones performed by Dunlop *et al* [13, 17]. This suggests that a strong ion-velocity effect exists in Ni.

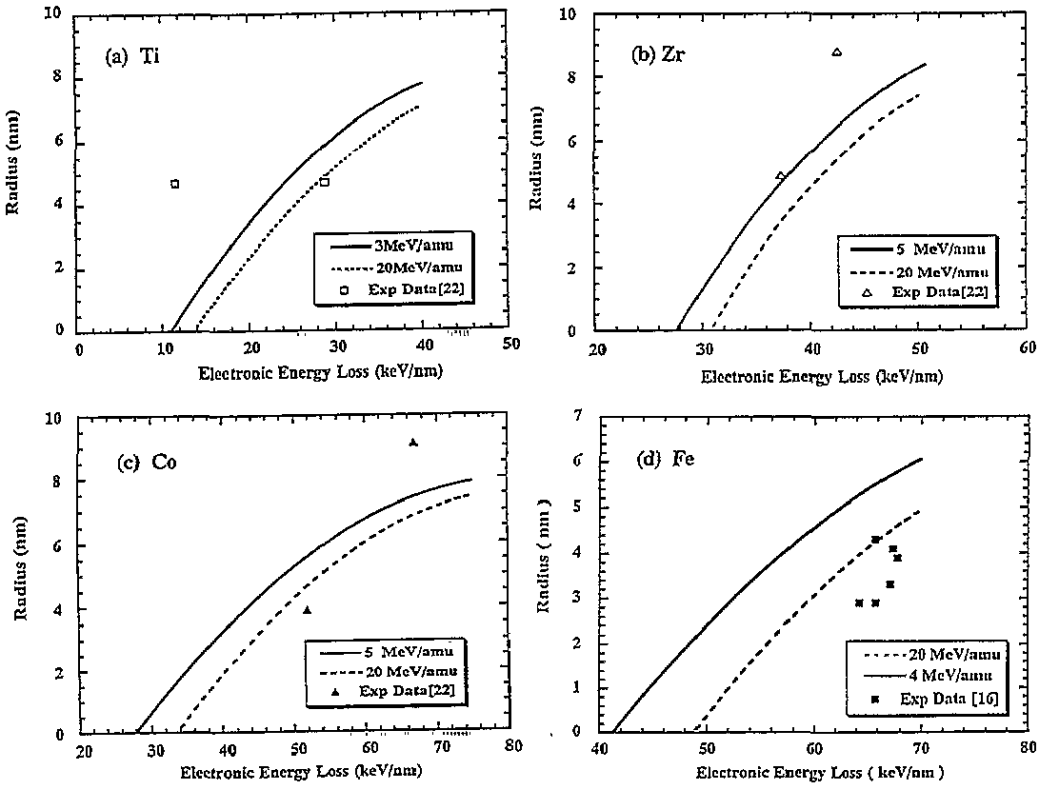

Figure 4. The radius of the molten phase versus S_e for different values of incident energy: comparisons between experimental track radii [16, 22] and calculated ones. In the calculations, we take into account the same valence number $z = 2(g(z) = g(z = 2))$. (*a*) Ti, $g = 9.28\times10^{12}$ W cm^{-3} K^{-1}; (*b*) Zr, $g = 3.50\times10^{12}$ W cm^{-3} K^{-1}; (*c*) Co, $g = 3.45\times10^{12}$ W cm^{-3} K^{-1} and (*d*) Fe, $g = 4.98\times10^{12}$ W cm^{-3} K^{-1}.

3.4. Experimentally S_e-insensitive metals

The study of sensitive metals allowed us to clarify the definition and the influence of all the parameters. In this section we extend our calculations to metals known as insensitive or nearly insensitive to the electronic slowing down such as Al, Cu, Nb, Ag, Pt and Pd [13, 17]. In table 3 we report, for each of these metals, the calculated value of g at 300 K with $z = 2$, the maximum value of the electronic stopping power S_e, the maximum temperature T_{am} reached along the ion path and the ratio T_{am}/T_m, where T_m is the melting temperature. Except for Pt and Pd, we clearly see that these metals are S_e insensitive ($T_{am}/T_m \leqslant 1$) and their $S_{e_{cr}}$ values are higher than could be reached in high-energy U-ion irradiations. For Pd, within the uncertainties of the input parameters, we may not conclude whether this metal is S_e sensitive or not.

4. Discussion of the E–P coupling g

Apart from the number $n_e = zn_a$ of valence electrons, which is taken as $z = 2$, g depends on two main physical parameters according to the formula developed in subsection 2.2.4: the Debye temperature linked to the sound velocity v and the thermal conductivity are very

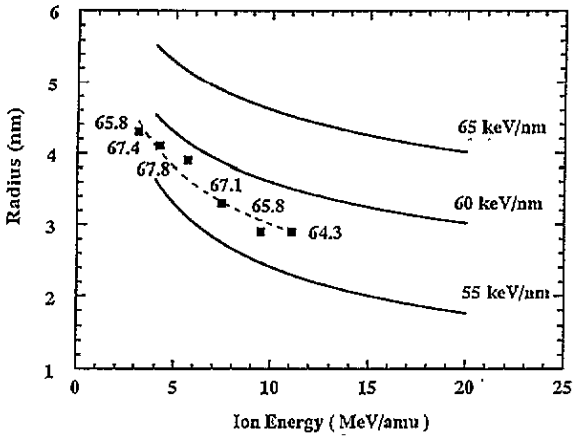

Figure 5. The ion-velocity effect in Fe. Each line corresponds to the radius evolution versus ion energy for the quoted value of S_e. The experimental radii data are from [16]. The theoretical curves are from the calculations with $g = g(z = 2) = 4.98 \times 10^{12}$ W cm^{-3} K^{-1}.

Table 3. Theoretical evolutions for some selected metals, using $g(z) = g(z = 2)$ and the S_e value at 5 MeV amu^{-1} U-ion irradiation. T_m is the melting temperature, T_{am} is the maximum value of lattice temperature and $S_{e_{cr}}$ is a hypothetical threshold value of defect creation.

Metal	g ($\times 10^{11}$) (W cm^{-3} K^{-1})	S_e (TRIM91) (keV nm^{-1})	T_{am} (K)	T_{am}/T_m
Al	8.1	28	763	0.82
Cu	5.0	70	713	0.53
Nb	15	63	2571	0.94
Ag	1.3	67	394	0.32
Pt	10	108	2045	1.00
Pd	14	80	1862	1.02

important. In order to investigate the influence of these two physical parameters, we have studied three specific cases as compared to Cu, which is S_e insensitive.

4.1. Beryllium

The thermal spike should not be efficient in Be because of its high melting point (1560 K) and high thermal conductivity, but this metal shows a high Debye temperature, which is four times that of Cu, and hence a high E–P coupling. It is then worth seeing if Be should be sensitive to S_e or not: the calculation shows that Be should be S_e sensitive ($S_{e_{cr}} \sim 11$ keV nm^{-1} for $z = 2$).

4.2. Gallium

Although the Debye temperature is nearly the same as that of Cu, this metal has all the characteristics of a very sensitive material because of its very low melting point (303 K), its low thermal conductivity (table 1) and its specific volume, larger in the liquid phase than in the solid state. Its E–P coupling is four times larger than that of Cu. Experimental irradiations have been performed [23–25]. The authors have pointed out that the interpretation of results was difficult. The calculation shows that Ga is very sensitive to S_e ($S_{e_{cr}} \sim 5$ keV nm^{-1} for $z = 2$).

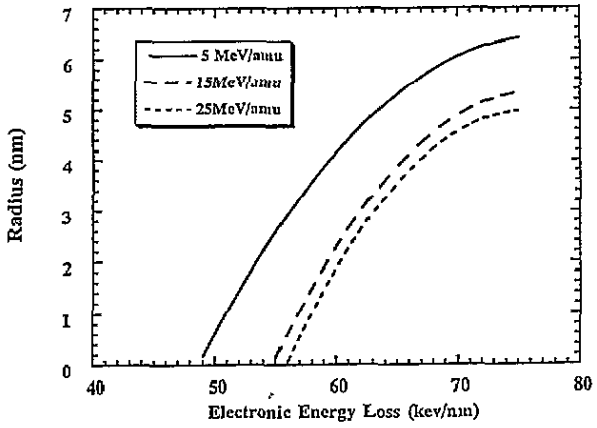

Figure 6. Variation of track radii in Ni with the incident-ion energy. The E–P coupling factor $g(z) = g(z = 2) = 4.05 \times 10^{12}$ W cm^{-3} K^{-1}; the initial target temperature $T_0 = 10$ K.

4.3. Nickel

The physical characteristics of Ni are very close to those of Cu. The main differences between Ni and Cu concern their thermal conductivity K(Ni) < K(Cu) and their Debye temperatures T_D(Ni) > T_D(Cu). Therefore the E–P coupling (deduced from (3″), $z = 2$) of Ni is much higher than that of Cu: $g_{Ni}(300\ K) = 4.3 \times 10^{12}$ W cm^{-3} K^{-1} whereas $g_{Cu}(300\ K) = 5.1 \times 10^{11}$ W cm^{-3} K^{-1}. We have already shown that materials are more S_e sensitive when their E–P coupling is high. The behaviour of Ni confirms this fact: it has been found sensitive from the point of view of defect annealing in contrast to Cu, which is insensitive to S_e [10–12]. In the present model, defect creation in Ni should appear for $S_e > 49$ keV nm^{-1} for the lowest incident-ion energy (figure 6). As compared to experiments [17], such a result needs discussion. With Pb ions at 20 MeV amu^{-1} ($S_e = 56$ keV nm^{-1}) there is no effect, in agreement with the calculation, but at 10 MeV amu^{-1} ($S_e = 67$ keV nm^{-1}) the calculation implies a defect creation, while in the experiment there is only defect annealing [17]. Taking into account the lack of precision of the input parameters in the model, this contradiction is not astonishing. However, the calculation suggests that Ni could be sensitive to S_e in an extreme case: a U beam at 5 MeV amu^{-1}.

5. Conclusion

The aim of this paper was to show that the behaviour of metals under irradiation by swift heavy ions is well correlated to the thermal-spike predictions. We conclude that the S_e sensitivity of a metal is closely linked to the following main properties.

(i) The melting point T_m: the lower the T_m, the lower the energy required to melt the material and hence the higher the sensitivity to S_e.

(ii) The E–P coupling g, proportional to T_D^2, z^2 and $1/K_e$ where T_D, z and K_e are respectively the Debye temperature, the number of valence electrons and the thermal conductivity. The larger the E–P coupling g, the higher the sensitivity to S_e. Using $z = 2$, we have been able to predict the sensitivity of metals to the electronic slowing down S_e. Our theoretical classification in S_e-sensitive and insensitive metals corresponds to the experimental data.

Table 4. Prediction of S_e sensitivities for some selected metals. ΔH_f is the energy required to melt a metal, S_e is the maximum value that can be reached in irradiations. The E–P coupling factor is a mean value and λ is the electron mean free path. The S_e^* values are the maximum S_e values that have been used in experiments.

Metal	ΔH_f (J cm^{-3})	S_e (TRIM91) (keV nm^{-1})	g ($\times 10^{11}$) (W cm^{-3} K^{-1})	λ (10^{-7} cm)	η	S_e effect	Measured S_e effect
Be	9368	23	293	3.92	5.2	Yes	
Mg	2270	20	6.82	21.6	0.61	No	
Al	3275	28	8.14	20.9	0.63	No	No [38] $S_e^* \leqslant 15$ keV/nm
Ti	6701	42	92.8	6.14	5.4	Yes	Yes [22]
V	8907	52	66.4	7.56	3.3	Yes	
Cr	9075	63	94.0	6.51	5.3	Yes	
Mn	7042	63	444	2.98	32	Yes	
Fe	10977	70	49.8	8.97	2.6	Yes	Yes [13]
Co	12199	75	34.5	10.9	1.7	Yes	Yes [22]
Ni	10529	77	40.5	10.1	2.2	Yes	No [13, 17] $S_e^* \leqslant 67$ keV nm^{-1}
Cu	6895	73	4.94	28.5	0.42	No	No [13] $S_e^* \leqslant 65$ keV nm^{-1}
Ga	1061	46	19.6	13.1	8.1	Yes	Yes [23]
Zr	4873	48	35.0	9.55	3.5	Yes	Yes [22]
Nb	9074	63	15.0	15.2	0.97	No	No [13] $S_e^* \leqslant 62$ keV nm^{-1}
Pd	7616	81	13.9	16.4	1.3	Yes?	No [17] $S_e^* < 75$ keV nm^{-1}
Ag	4118	70	1.26	53.1	0.19	No	No [13, 17] $S_e^* \leqslant 68$ keV nm^{-1}
Sn	1184	45	3.69	28.7	1.5	Yes	
W	14011	93	12.4	17.0	0.74	No	No [17] $S_e^* \leqslant 80$ keV nm^{-1}
Pt	9003	109	10.3	18.9	1.1	No	No [13] $S_e^* \leqslant 90$ keV nm^{-1}
Au	4443	99	0.91	62.5	0.18	No	
Pb	1109	55	1.56	43.3	0.85	No	
Bi	1136	50	8.20	18.4	4.2	Yes	Yes [19]
U	3149	95	12.4	16.3	3.7	Yes	

In order to predict the S_e sensitivity of a metal, it is clear that many physical parameters must be first collected and then a rather long calculation must be performed, so we find out one characteristic that could quickly show the sensitivity of a metal to the electronic slowing down. This characteristic could be the mean energy density Q deposited in the lattice in a cylinder of radius λ which is the characteristic length of the energy distribution. In such a cylinder 63% of the S_e is involved and:

$$Q = 0.63 S_e / \pi \lambda^2. \tag{4}$$

λ is taken from [29] and is the electron mean free path linked to the thermal electronic diffusivity $D_e(T_e)$ and to the E–P interaction time τ_a by $\lambda^2 = D_e \tau_a$. In the present formalism, $\tau_a = C_e(T_e)/g$. Hence $\lambda^2 = K(T)/g$ is calculated at $T_e = T_a = 300$ K. In table 4, we compare for several metals this energy density Q to the energy ΔH_f required to melt the corresponding metal. We analyse the ratio $\eta = Q/\Delta H_f$ as follows.

If $\eta > 1.3$, the material must be S_e sensitive; if $\eta < 0.7$, the material must be S_e insensitive. In the intermediate range $0.7 \leqslant \eta \leqslant 1.3$, the lack of precision of the input parameters does not allow any definitive conclusion. Table 4 also confirms the fact

that thermodynamic point of view gives a satisfactory explanation of the behaviour of metals under irradiation. Such a phenomenological approach can be used whatever the metal provided that the Debye temperature and the thermal conductivity are known. The remaining uncertainties originate from the number of valence electrons participating in the hot electronic conduction: the value of $z = 2$ deduced for transition metals has to be checked in other irradiated metals.

Appendix

From [55–58], we show some physical parameters of the selected metals in tables A1 and A2 as follows.

Table A1. Physical data of the metals used in the theoretical calculations. T_m, T_v, ρ_s, ρ_l, n_a, H_f and H_v are respectively the melting temperature, vaporization temperature, solid density, liquid density, atomic density at room temperature and latent heats of melting and vaporization.

Metal	T_m (K)	T_v (K)	ρ_s (g cm^{-3})	ρ_l (g cm^{-3})	n_a (10^{22} cm^{-3})	H_f (J cm^{-3})	H_v (J cm^{-3})
Be	1560	2745	1.85	1.690	12.1	2504	60 023
Mg	923	1363	1.74	1.585	4.30	658	9426
Al	933	2740	2.70	2.368	6.02	1075	28 403
Ti	1933	3560	4.51	4.11	5.66	1810	36 225
Fe	1809	3135	7.86	7.015	8.48	1942	49 203
Co	1768	3143	8.9	7.67	8.97	2336	58 707
Ni	1726	3005	8.91	7.905	9.14	2671	57 398
Cu	1356	2840	8.93	7.940	8.45	1827	38 022
Ga	303	2676	5.904	6.095	5.10	474	22 383
Zr	2125	4650	6.51	5.80	4.29	1074	26 578
Nb	2741	5015	8.58	7.83	5.56	2239	57 478
Pd	1825	3413	12.0	10.70	6.80	1942	37 412
Ag	1234	2485	10.5	9.33	5.85	1162	21 953
Pt	2045	4100	21.47	18.91	6.62	2392	49 430
Bi	544	1837	9.81	10.02	2.84	530	4913

Table A2. The lattice specific heat C and thermal conductivity K of selected metals used in the theoretical calculations. The formulas describing the temperature dependence of C and K are deduced from the measured data.

Metal	Temperature range	Lattice specific heat C (J g^{-1} K^{-1}) and thermal conductivity K (W cm^{-1} K^{-1})
Be	10–293 K	$C = 0.0055 - 0.000\,90T + 2.6 \times 10^{-5}T^2$
	293–1560 K	$C = 1.51 + 0.0016T - 2.3 \times 10^{-7}T^2$
	$T > 1560$ K	$C = 3.5$
	$T < 20$ K	$K = 30$
	20–293 K	$K = 35.3 - 0.30T + 0.000\,94T^2 - 1.0 \times 10^{-6}T^3$
	293–1560 K	$K = 0.56 + 1.2 \times 10^3 T^{-1.19}$
	$T > 1560$ K	$K = 0.74$
Mg	10–100 K	$C = 0.062 - 0.0094T + 0.000\,41T^2 - 3.6 \times 10^{-6}T^3 + 9.8 \times 10^{-9}T^4$
	100–300 K	$C = -0.22 + 0.013T - 4.8 \times 10^{-5}T^2 + 6.4 \times 10^{-8}T^3$
	300 K–T_m	$C = 0.72 + 0.0015T - 2.0 \times 10^{-6}T^2 + 1.2 \times 10^{-9}T^3$
	$T > T_m$	$C = 1.36$
	10–30 K	$K = -3.94 + 2.67T - 0.11T^2 + 0.0013T^3$
	30–300 K	$K = 1.52 + 1.36 \times 10^4/(T + 11)^2$
	300 K–T_m	$K = 0.90 + 0.0049T - 9.0 \times 10^{-6}T^2 + 3.8 \times 10^{-9}T^3$

Table A2. (continued)

Metal	Temperature range	Lattice specific heat C (J g^{-1} K^{-1}) and thermal conductivity K (W cm^{-1} K^{-1})
	T_m–T_v	$K = 0.20 + 6.3 \times 10^{-4}T$
	$T > T_v$	$K = 1.06$
Al	10–100 K	$C = 0.032 - 0.0045T + 0.000\,18T^2 - 8.7 \times 10^{-7}T^3$
	100–300 K	$C = -0.34 + 0.012T - 4.0 \times 10^{-5}T^2 + 5.0 \times 10^{-8}T^3$
	300–700 K	$C = 0.76 + 4.6 \times 10^{-4}T$
	$T > 700$ K	$C = 1.08$
	6–15 K	$K = -4.04 + 9.67T - 0.32T^2$
	15–100 K	$K = 146.5 - 6.8T + 0.12T^2 - 0.0010T^3 + 3.8 \times 10^{-6}T^4$
	100–300 K	$K = 8.84 - 0.11T + 7.5 \times 10^{-4}T^2 - 2.2 \times 10^{-6}T^3 + 2.4 \times 10^{-9}T^4$
	300–T_m	$K = 2.4$
	T_m–T_v	$K = 0.63 + 3.3 \times 10^{-4}T$
	$T > T_v$	$K = 1.5$
Ti	10–100 K	$C = 0.015 - 0.0024T + 0.000\,11T^2 - 5.8 \times 10^{-7}T^3$
	100–300 K	$C = -0.088 + 0.0056T - 1.8 \times 10^{-5}T^2 + 2.2 \times 10^{-8}T^3$
	300 K–T_m	$C = 0.41 + 0.000\,40T - 1.5 \times 10^{-7}T^2 + 9.5 \times 10^{-12}T^3$
	$T > T_m$	$C = 0.70$
	4–30 K	$K = -0.0075 + 0.014T - 1.5 \times 10^{-4}T^2 + 2.0 \times 10^{-6}T^3$
	30–100 K	$K = 0.13 + 0.10T - 0.000\,14T^2 + 5.0 \times 10^{-7}T^3 - 1.3 \times 10^{-9}T^4$
	100–300 K	$K = 0.53 - 0.0025T + 5.3 \times 10^{-6}T^2 - 3.7 \times 10^{-9}T^3$
	300–T_m	$K = 0.13 + 5.3 \times 10^{-5}T - 1.4 \times 10^{-7}T^2 + 1.6 \times 10^{-10}T^3 - 4.0 \times 10^{-14}T^4$
	$T > T_m$	$K = 0.28$
Fe	10–100 K	$C = 0.17 - 0.0020T + 7.3 \times 10^{-5}T^2 - 3.3 \times 10^{-7}T^3$
	100–300 K	$C = -0.20 + 0.0060T - 2.0 \times 10^{-5}T^2 + 2.5 \times 10^{-8}T^3$
	300–1073 K	$C = 0.32 + 4.3 \times 10^{-4}T + 1.4 \times 10^{-8}T^2$
	1073 K–T_m	$C = 0.79 + 5.4 \times 10^{-6}T$
	$T > T_m$	$C = 0.80$
	1–20 K	$K = -0.45 + 0.97T - 0.022T^2$
	20–100 K	$K = 16.5 - 0.35T + 0.0020T^2$
	100–T_m	$K = 1.24 - 0.0017T + 8.8 \times 10^{-7}T^2 - 1.3 \times 10^{-10}T^3$
	$T > T_m$	$K = 0.33$
Co	10–293 K	$C = 0.36 + 2.4 \times 10^{-4}T$
	293–1500 K	$C = 0.22 + 0.0013T - 2.6 \times 10^{-6}T^2 + 2.5 \times 10^{-9}T^3 - 7.6 \times 10^{-13}T^4$
	$T > 1500$ K	$C = 0.88$
	10–20 K	$K = -0.73 + 0.48T - 0.016T^2$
	20–273 K	$K = 7.7 - 0.14T + 0.0012T^2 - 4.5 \times 10^{-6}T^3 + 6.0 \times 10^{-9}T^4$
	273–T_m	$K = 2.3 - 0.0055T + 6.5 \times 10^{-6}T^2 - 3.6 \times 10^{-9}T^3 + 7.5 \times 10^{-13}T^4$
	$T > T_m$	$K = 0.42$
Ni	10–100 K	$C = 0.016 - 0.0021T + 8.3 \times 10^{-5}T^2 - 4.1 \times 10^{-7}T^3$
	100–300 K	$C = -0.16 + 0.0056T - 1.9 \times 10^{-5}T^2 + 2.5 \times 10^{-8}T^3$
	300 K–T_m	$C = 0.39 + 0.000\,19T - 3.3 \times 10^{-8}T^2 + 3.8 \times 10^{-11}T^3$
	$T > T_m$	$C = 0.62$
	10–100 K	$K = 58.2 - 1.5T + 0.013T^2 - 3.5 \times 10^{-5}T^3$
	100–T_m	$K = 3.4 - 0.013T + 2.2 \times 10^{-5}T^2 - 1.5 \times 10^{-8}T^3 + 3.6 \times 10^{-12}T^4$
	$T > T_m$	$K = 0.50$
Cu	10–100 K	$C = 0.0058 - 0.0015T + 9.3 \times 10^{-5}T^2 - 5.3 \times 10^{-7}T^3$
	100–300 K	$C = -0.053 + 0.0046T - 1.7 \times 10^{-5}T^2 + 2.2 \times 10^{-8}T^3$
	300 K–T_m	$C = 0.36 + 8.6 \times 10^{-5}T + 2.9 \times 10^{-9}T^2$
	$T > T_m$	$C = 0.50$
	4–15 K	$K = 22.6 + 9.2T + 1.0T^2 - 0.079T^3$
	15–100 K	$K = 287 - 15T + 0.31T^2 - 0.0029T^3 + 9.7 \times 10^{-6}T^4$
	100–300 K	$K = 6.7 - 0.035T + 1.5 \times 10^{-4}T^2 - 2.0 \times 10^{-7}T^3$
	300 K–T_m	$K = 3.9 + 0.0013T - 3.0 \times 10^{-6}T^2 + 9.2 \times 10^{-10}T^3$
	T_m–2000 K	$K = 0.60 + 0.0011T - 2.6 \times 10^{-7}T^2$
	$T > 2000$ K	$K = 2.1$

Table A2. (continued)

Metal	Temperature range	Lattice specific heat C (J g^{-1} K^{-1}) and thermal conductivity K (W cm^{-1} K^{-1})
Ga	$T < 50$ K	$C = 1.24 \times 10^{-6}T^3$
	$T > 50$ K	$C = -0.18 + 0.52[1 - \exp(-0.0195T)]$
	$T > T_m$	$C = 0.40$
	$T < 30$ K	$K = 1989T^{-1.9}$
	$T > 30$ K	$K = 64T^{-0.885}$
	$T > T_m$	$K = 0.00043T + 0.13$
	$T > T_v$	$K = 0.80$
Zr	10–273 K	$C = 0.23$
	273 K–T_m	$C = 0.28 - 0.00022T + 1.2 \times 10^{-7}T^2$
	$T > T_m$	$C = 0.37$
	10–100 K	$K = -0.078 + 0.16T - 0.0061T^2 + 7.8 \times 10^{-5}T^3 - 3.3 \times 10^{-7}T^4$
	100 K–T_m	$K = 0.28 - 0.00051T + 6.0 \times 10^{-7}T^2 - 1.7 \times 10^{-10}T^3$
	$T > T_m$	$K = 0.34$
Nb	10–100 K	$C = 0.016 - 0.0029T + 1.7 \times 10^{-4}T^2 - 1.9 \times 10^{-6}T^3 + 7.0 \times 10^{-9}T^4$
	100–300 K	$C = 0.038 + 0.0025T - 9.4 \times 10^{-6}T^2 + 1.2 \times 10^{-8}T^3$
	300–1273 K	$C = 0.25 + 4.4 \times 10^{-5}T + 9.6 \times 10^{-10}T^2$
	$T > 1273$ K	$C = 0.31$
	4–25 K	$K = 0.019 + 0.065T - 0.0012T^2$
	25–100 K	$K = 1.12 - 0.0020T - 3.8 \times 10^{-4}T^2 + 6.0 \times 10^{-6}T^3 - 2.5 \times 10^{-8}T^4$
	100–273 K	$K = 0.51$
	273 K–T_m	$K = 0.58 - 0.00047T + 5.8 \times 10^{-7}T^2 - 3.2 \times 10^{-10}T^3 + 6.3 \times 10^{-14}T^4$
	$T > T_m$	$K = 0.64$
Pd	10–100 K	$C = 0.016 - 0.0026T + 0.00014T^2 - 1.6 \times 10^{-6}T^3 + 5.7 \times 10^{-9}T^4$
	100–300 K	$C = 0.014 + 0.0013T - 4.8 \times 10^{-6}T^2 + 6.3 \times 10^{-9}T^3$
	300–1300 K	$C = 0.23 + 5.5 \times 10^{-5}T$
	$T > 1300$ K	$C = 0.30$
	10–100 K	$K = 14.2 - 0.40T + 0.0038T^2 - 1.1 \times 10^{-5}T^3$
	100–300 K	$K = 1.8 - 0.013T + 5.0 \times 10^{-5}T^2 - 6.6 \times 10^{-8}T^3$
	300–1300 K	$K = 0.77 - 0.00053T + 8.9 \times 10^{-7}T^2 - 3.7 \times 10^{-10}T^3$
	$T > 1300$ K	$K = 0.78$
Ag	10–100 K	$C = 0.0090 - 0.0023T + 1.8 \times 10^{-4}T^2 - 2.3 \times 10^{-6}T^3 + 9.2 \times 10^{-9}T^4$
	100–300 K	$C = 0.084 + 0.0015T - 5.2 \times 10^{-6}T^2 + 6.5 \times 10^{-9}T^3$
	300 K–T_m	$C = 0.25 - 6.8 \times 10^{-5}T + 5.2 \times 10^{-8}T^2$
	$T > T_m$	$C = 0.28$
	10–50 K	$K = 330 - 23T + 0.57T^2 - 0.046T^3$
	50–100 K	$K = 29.3 - 0.85T + 0.0095T^2 - 3.6 \times 10^{-5}T^3$
	100–300 K	$K = 4.0$
	300 K–T_m	$K = 3.5 + 0.0034T - 3.9 \times 10^{-6}T^2$
	T_m–T_v	$K = 1.2 + 0.00043T$
	$T > T_v$	$K = 2.3$
Pt	10–100 K	$C = -0.012 + 0.0021T^{0.863}$
	100–300 K	$C = 0.014 + 0.0013T - 4.8 \times 10^{-6}T^2 + 6.3 \times 10^{-9}T^3$
	300 K–T_m	$C = 0.13 + 1.0 \times 10^{-5}T + 2.7 \times 10^{-8}T^2 - 9.6 \times 10^{-12}T^3$
	$T > T_m$	$C = 0.18$
	10–100 K	$K = 24.6 - 0.98T + 0.14T^2 - 5.9 \times 10^{-5}T^3$
	100–300 K	$K = 1.5 - 0.0089T + 3.6 \times 10^{-5}T^2 - 5.0 \times 10^{-8}T^3$
	300 K–T_m	$K = 0.74 - 3.8 \times 10^{-4}T + 4.3 \times 10^{-7}T^2 - 1.7 \times 10^{-10}T^3 + 1.2 \times 10^{-14}T^4$
	$T > T_m$	$K = 0.68$
Bi		See [19]

References

[1] Lesueur D 1975 *Radiat. Eff.* **24** 101

[2] Klaumunzer S and Schumacher G 1983 *Phys. Rev. Lett.* **51** 1987

[3] Klaumunzer S, Hou Ming-dong and Schumacher G 1986 *Phys. Rev. Lett.* **57** 850

[4] Hou Ming-dong, Klaumunzer S and Schumacher G 1990 *Phys. Rev.* B **41** 1144
[5] Audouard A, Balanzat E, Fuchs G, Jousset J C, Lesueur D and Thomé L 1987 *Europhys. Lett.* **3** 327
[6] Audouard A, Balanzat E, Fuchs G, Jousset J C, Lesueur D and Thomé L 1988 *Europhys. Lett.* **5** 241
[7] Audouard A, Balanzat E, Bouffard S, Jousset J C, Chamberod A, Dunlop A, Lesueur D, Fuchs G, Spohr R, Vetter J and Thomé L 1990 *Phys. Rev. Lett.* **65** 875
[8] Barbu A, Dunlop A, Henry J, Lesueur D and Lorenzelli N 1992 *Mater. Sci. Forum* **97–99** 577
[9] Barbu A, Dunlop A, Lesueur D and Averback R S 1991 *Europhys. Lett.* **15** 3713
[10] Iwase A, Sasaki S, Iwata T and Nihira T 1988 *J. Nucl. Mater.* **155–157** 1188
[11] Iwase A, Iwata T, Sasaki S and Nihira T 1990 *J. Phys. Soc. Japan* **59** 1451
[12] Iwase A, Sasaki S, Iwata T and Nihira T 1987 *Phys. Rev. Lett.* **58** 2450
[13] Dunlop A and Lesueur D 1993 *Radiat. Eff. Defects Solids* **126** 123
[14] Dunlop A, Lesueur D, Morillo J, Dural J, Spohr R and Vetter J 1989 *C. R. Acad. Sci., Paris II* **309** 1277
[15] Dunlop A, Lesueur D and Dural J 1989 *Nucl. Instrum. Methods Res.* B **42** 182
[16] Dunlop A, Lesueur D, Morillo J, Dural J, Spohr R and Vetter J 1990 *Nucl. Instrum. Methods Res.* B **48** 419
[17] Dunlop A, Legrand P, Lesueur D, Lorenzelli N, Morillo J, Barbu A and Bouffard S 1991 *Europhys. Lett.* **15** 765
[18] Dimitrov C, Legrand P, Dunlop A and Lesueur D 1992 *Mater. Sci. Forum* **97–99** 593
[19] Dufour C, Audouard A, Beuneu F, Dural J, Girard J P, Hairie A, Levalois M, Paumier E and Toulemonde M 1993 *J. Phys.: Condens. Matter* **5** 4573
[20] Dammak H, Barbu A, Dunlop A, Lesueur D and Lorenzelli N 1993 *Phil. Mag. Lett.* **67** 253
[21] Henry J, Barbu A, Leridon B, Lesueur D and Dunlop A 1992 *Nucl. Instrum. Methods Res.* B **67** 390
[22] Dammak H, Lesueur D, Dunlop A, Legrand P and Morillo J 1993 *Radiat. Eff. Defects Solids* **126** 111
[23] Paumier E, Toulemonde M, Dural J, Rullier-Albenque F, Girard J P and Bogdanski P 1989 *Europhys. Lett.* **10** 555
[24] Paumier E, Toulemonde M, Dural J, Girard J P, Bogdanski P, Dufour C, Carin R, Hairie A, Julienne D, Levalois M, Madelon R and Metzner M N 1992 *Mater. Sci. Forum* **97–99** 599
[25] Buckel W and Hilsch R 1954 *Z. Phys.* **138** 109
[26] Izui K and Furuno S 1986 *Proc. XI Int. Congress on Electron Microscopy (Kyoto, 1986)* ed T Imura, S Maruse and T Suzuki (Tokyo: Society of Electron Microscopy) p 1299
[27] Meftah A, Brisard F, Costantini J M, Hage-Ali M, Stoquert J P, Studer F and Toulemonde M 1993 *Phys. Rev.* B **48** 920
[28] Thibaudau F, Cousty J, Balanzat E and Bouffard S 1991 *Phys. Rev. Lett.* **67** 1582
[29] Toulemonde M, Dufour C and Paumier E 1992 *Phys. Rev.* B **46** 14362
[30] Desauer F 1923 *Z. Phys.* **12** 38
[31] Seitz F and Koehler J S 1956 *Solid State Physics* vol 2 (New York: Academic) p 305
[32] Lifshitz I M, Kaganov M I and Tanatarov L V 1960 *J. Nucl. Energy* A **12** 69
[33] Chadderton L T and Montagu-Pollock H 1969 *Proc. R. Soc.* A **274** 239
[34] Fleisher R L, Price P B and Walker R M 1965 *J. Appl. Phys.* **36** 3645
[35] Lesueur D and Dunlop A 1993 *Radiat. Eff. Defects Solids* **126** 163
[36] Legrand P, Morillo J and Pontikis V 1993 *Radiat. Eff. Defects Solids* **126** 151
[37] Iwase A, Iwata T and Nihira T 1992 *J. Phys. Soc. Japan* **61** 3878
[38] Iwase A, Sasaki S, Iwata T and Nihira T 1985 *J. Nucl. Mater.* **133/134** 365
[39] Audouard A, Balanzat E, Jousset J C, Chamberod A, Fuchs G, Lesueur D and Thomé L 1991 *Phil. Mag.* B **63** 727
[40] Thomé L, Garrido F, Dran J C, Benyagoub A, Klaumunzer S and Dunlop A 1992 *Phys. Rev. Lett.* **68** 808
[41] Allen P B 1987 *Phys. Rev. Lett.* **59** 1460
[42] Kaganov M I, Lifshitz I M and Tanatarov L V 1957 *Sov. Phys.–JETP* **4** 173
[43] Martynenko Yu V and Yavlinskii Yu N 1983 *Sov. Phys.–Dokl.* **28** 391
[44] Toulemonde M, Paumier E and Dufour C 1993 *Radiat. Eff. Defects Solids* **126** 201
[45] Dufour C, Paumier E and Toulemonde M 1993 *Radiat. Eff. Defects Solids* **126** 119
[46] Borson S D, Kazeroonian A, Moodera J S, Face D W, Cheng T K, Ippen E P, Dresselhaus M S and Dresselhaus G 1990 *Phys. Rev. Lett.* **64** 2172
[47] Brorson S D, Fujimoto J G and Ippen E P 1987 *Phys. Rev. Lett.* **59** 1962
[48] Ashcroft N W and Mermin N D 1976 *Solid State Physics* (New York: Holt, Reinhart and Winston)
[49] Lin W Z, Fujimoto J G, Ippen E P and Logan R A 1987 *Appl. Phys. Lett.* **50** 124
[50] Fujimoto J G, Liu J M, Ippen E P and Bloembergen N 1984 *Phys. Rev. Lett.* **53** 1837
[51] Tom H W K, Aumiller G D and Brito-Cruz C H 1988 *Phys. Rev. Lett.* **60** 1438
[52] Qiu T Q and Tien C L 1992 *Int. J. Heat Mass Transfer* **35** 719
[53] Izui K 1965 *J. Phys. Soc. Japan* **20** 915

[54] Milchberg H M, Freeman R R and Davey S C 1988 *Phys. Rev. Lett.* **61** 2364
[55] Kittel C 1983 *Physique de l'Etat Solide* 5th edn (Paris: Bordas)
[56] 1961 *Properties of Materials at Low Temperatures (Phase I), A Compendium* ed V J Johnson (Oxford: Pergamon)
[57] Brandes E A (ed) 1983 *Metals* 6th edn (London: Butterworths)
[58] Weast R C (ed) 1976–1977 *Handbook of Chemistry and Physics* 57th edn (Boca Raton, FL: Chemical Rubber Company)
Lide D R (ed) 1992–1993 *Handbook of Chemistry and Physics* 73rd edn (Boca Raton, FL: Chemical Rubber Company)
[59] Katz R and Kobetich E J 1968 *Phys. Rev.* **170** 397; 1969 *Phys. Rev.* **186** 344
[60] Gervais B 1993 *Thèse* Université de Caen
[61] Waligorski M P R, Hamm R N and Katz R 1986 *Nucl. Tracks Radiat. Meas.* **11** 309
[62] Dufour C 1993 *Thèse Rapport* CEA-R-5638
[63] Hubert F, Bimbot R and Gauvin H 1990 *At. Data Nucl. Data Tables* **46**
[64] Biersack J P and Haggmark L G 1980 *Nucl. Instrum. Methods Res.* **174** 257
[65] Ziegler J F 1980 *Handbook of 'Stopping Cross-Sections for Energetic Ions in all Elements' (The Stopping and Ranges of Ions in Matter 5)* (Oxford: Pergamon)